



This open access document is posted as a preprint in the Beilstein Archives at <https://doi.org/10.3762/bxiv.2022.28.v1> and is considered to be an early communication for feedback before peer review. Before citing this document, please check if a final, peer-reviewed version has been published.

This document is not formatted, has not undergone copyediting or typesetting, and may contain errors, unsubstantiated scientific claims or preliminary data.

**Preprint Title** Immunization of mice with gold nanoparticles conjugated to thermostable tumor antigens prevents tumor development during transplantation

**Authors** Sergey A. Staroverov, Sergey V. Kozlov, Alexander S. Fomin, Daniil S. Chumakov, Konstantin P. Gabalov, Yevgeny S. Kozlov, Dmitry A. Soldatov and Lev A. Dykman

**Publication Date** 26 Apr. 2022

**Article Type** Full Research Paper

**ORCID® iDs** Dmitry A. Soldatov - <https://orcid.org/0000-0003-2296-5770>; Lev A. Dykman - <https://orcid.org/0000-0003-2440-6761>

# **Immunization of mice with gold nanoparticles conjugated to thermostable tumor antigens prevents tumor development during transplantation**

Sergey A. Staroverov<sup>1,2</sup>, Sergey V. Kozlov<sup>2</sup>, Alexander S. Fomin<sup>1</sup>, Daniil S. Chumakov<sup>1</sup>, Konstantin P. Gabalov<sup>1</sup>, Yevgeny S. Kozlov<sup>2</sup>, Dmitry A. Soldatov<sup>2</sup>, Lev A. Dykman\*<sup>1</sup>

Address: <sup>1</sup>Institute of Biochemistry and Physiology of Plants and Microorganisms, Saratov Scientific Centre of the Russian Academy of Sciences, Prospekt Entuziastov 13, Saratov, 410049 Russia

<sup>2</sup>Vavilov Saratov State Agrarian University, Teatralnaya Ploshchad 1, Saratov, 410012 Russia

\* Corresponding author: Lev A. Dykman - email: dykman\_l@ibppm.ru

## **Abstract**

Gold nanoparticles as part of vaccines greatly increase antigen stability, antigen accumulation in the lymph nodes, and antigen uptake by antigen-presenting cells.

The use of such particles as part of anticancer vaccines based on heat shock proteins to increase vaccine effectiveness is timely. We prepared and characterized nanoconjugates based on 15-nm gold nanoparticles and thermostable tumor antigens isolated from MH22a murine hepatoma cells. BALB/c mice were injected with the conjugates and then received transplants of MH22a cells. The immunized

mice showed no signs of tumor growth for 24 days. They also showed decreased production of the INF- $\gamma$ , IL-6, and IL-1 proinflammatory cytokines, as compared to the mice immunized through other schemes. This study is the first to show that it is possible in principle to use gold nanoparticles in combination with thermostable tumor antigens for antitumor vaccination. Antitumor vaccines based on thermostable tumor antigens can be largely improved by including gold nanoparticles as additional adjuvants.

## **Keywords:**

Gold nanoparticles; heat shock proteins; vaccination; adjuvant; tumor transplantation

## **Introduction**

Immunotherapy of malignant tumors is an important biomedical research area. In time it may take its place alongside surgery, chemotherapy, and radiotherapy as a standard in cancer treatment. Current cancer immunotherapies include cytokine therapy [1], immune-checkpoint inhibition [2], adaptive cell therapy [3], and antitumor vaccines [4].

Anticancer vaccines stimulate antitumor immunity. The basic idea behind such vaccines is that malignant cells overexpress tumor antigens to which a T-cell immune response can be mounted. Any antitumor vaccine includes the following elements:

(1) an antigen, (2) a carrier, which determines the delivery of the antigen to the lymphoid organs, (3) an adjuvant, which enhances the immunogenicity of the antigen [5]. Whether this approach is successfully transferred from laboratory to clinic depends critically on the overcoming of the associated problems. First, the administered vaccine may accumulate poorly in lymph nodes. Second, the antigen

may be inefficiently processed and presented by dendritic cells. This prevents the induction of a sufficient CD8<sup>+</sup> T-cell response [6].

Nanoscale materials can help to solve these problems. Organic and inorganic nanoparticles in tumor vaccines greatly increase the stability of an antigen and its accumulation in lymph nodes, uptake, processing, and cross-presentation by antigen-presenting cells [7-9]. Among all available nanoparticles, gold nanoparticles (GNPs) excel for this purpose [10]. They act both as an antigen carrier and as an adjuvant [11]. GNPs are chemically inert, biocompatible, and easy to make. In addition, their surface can easily be functionalized with biomolecules, including antigens of various natures [12,13]. The unique plasmon resonance properties of GNPs make it possible to track the biodistribution of GNP-based vaccines and develop multimodal nanocomposites, which combine efficient antigen delivery with photothermal activity and imaging possibility [14]. GNPs are popularly used to design antibacterial, antiviral, and antiparasitic vaccines [15,16].

The work of Brinas et al. was one of the first to report on the induction in laboratory animals of an immune response to tumor antigens conjugated to colloidal gold without the use of additional adjuvants. The authors used GNPs conjugated to a glycopeptide antigen based on the MUC4 mucin, a modified Thomsen–Friedenreich antigen, and a peptide from the complement-derived protein C3d. Twelve weeks after the vaccination, there was a statistically significant increase in the blood content of IgG and IgM antibodies [17]. Parry et al. reported the preparation of antibodies specific to the tumor monosaccharide Tn-antigen without the use of conventional protein components of vaccines. Animals were immunized with GNPs conjugated to a polymerized Tn-antigen [18]. Cai et al. showed that animals immunized with PEGylated GNPs conjugated to a glycopeptide sequence derived from MUC1 and the T-cell epitope P30 sequence developed Th1 and Th2 immune responses. The

resultant antiserum contained antibodies that recognized MUC-1 molecules on the surface of MCF-7 breast cancer cells [19]. In vitro, GNPs complexed with MUC-1 mucin increased the production of the TNF- $\alpha$ , IL-6, IL-10, and IL-12 cytokines by peritoneal macrophages and induced macrophage polarization [20]. In addition, GNPs coupled to the adjuvant of  $\alpha$ -galactosylceramide was used to enhance immune response to MUC-1 [21].

Almeida et al. experimentally validated a GNP-based peptide antitumor nanovaccine. GNPs coated with the ovalbumin epitope were injected subcutaneously into mice. The animals injected with the conjugate showed a significant increase in INF- $\gamma$  production by splenocytes. Seven days after the last immunization, the animals were challenged with B16-OVA melanoma cells. The immunized animals survived 100% within 50 days of the experiment [22]. Ahn et al. studied the response of RAW 264.7 macrophages and of dendritic and T cells isolated from mice to GNPs conjugated to peptides derived from tumor cell antigens. The GNP-peptide complexes induced 15-fold higher TNF- $\alpha$  production by macrophages than did the free antigen. The complexes also enhanced antigen cross-presentation by dendritic cells, which was manifested as increased elaboration of IFN- $\gamma$  and IL-2 by T-lymphocytes [23].

GNPs are also used as a carrier in the development of antitumor DNA vaccines. Specifically, Gulla et al. used 24-nm gold nanospheres conjugated to the DNA sequence encoding the MART1 melanoma antigen (pCMV-MART1) to immunize mice and examine their response to subsequent tumor-cell transplantation.

Additionally, the authors coated the nanoconjugates with a mannose-mimicking shikimoyl ligand to target dendritic cells and a guanidinylligand to facilitate transfection. The nanovaccine-immunized mice survived the entire experimental period (180 days) without tumor signs after subcutaneous melanoma transplantation. Cytotoxic lymphocyte depletion studies showed that CD8<sup>+</sup> T-lymphocytes are the key

link in the antitumor immune response when the nanoconjugates are injected [24].

Also of note are works in which GNPs were used as a siRNA carrier to inhibit immune response checkpoints [25,26]. Thus, GNPs are promising candidates for improving the efficacy and safety of cancer immunotherapy [27].

Heat shock proteins (HSPs) can play an important part in the induction of an antitumor adaptive immune response [28]. HSPs are primarily known as highly conserved chaperone proteins involved in the folding, assembly, and disassembly of protein complexes [29]. Their chaperone activity, in fact, underlies the mediation of efficient capture, processing, and cross-presentation of tumor peptide antigens by dendritic cells [30]. On the other hand, HSPs can also modulate the innate immune response by participating in NK cell activation [31]. They promote the production of chemokines and such pro- and antiinflammatory cytokines as IL-1, IL-6, IL-10, IL-12, TNF- $\alpha$ , and IFN- $\gamma$  [32,33]. Thermostable proteins of the HSP family have been popularly used as adjuvants in the design of vaccines against a variety of cancers [34-36]. Some of these developments have reached phase III trials [37]. Phase I and II trials of therapeutic vaccines containing HSP-peptide complex-96 (HSPPC-96) for glioblastoma treatment are under way [38].

In the use of HSP-based vaccines, the immune response can be enhanced with nanoscale materials. Shevtsov et al. coupled iron oxide nanoparticles to recombinant HSP 70 for orthotopic experimental glioblastoma therapy in animals. Seven days after tumor cell transplantation, the animals were immunized with a mixture of dendritic cells, tumor antigens derived from the lysate, and nanoconjugates. The animals in the experimental group showed significant inhibition of tumor growth and activation of CD8<sup>+</sup> T-cell response, as compared to the group immunized with a nanoparticle-free dendritic cell-HSP 70-antigen mixture [39].

There is no literature on the use of GNPs in combination with HSPs for antitumor vaccination. We investigated the part GNPs play in the induction of antitumor immunity in laboratory mice.

## Results

### Characterization of GNPs

The absorption spectrum peak of the resultant sol was  $\lambda_{\max} = 518$  nm, and the absorbance in a 1-cm-path-length cuvette was  $A_{518} = 1.1$ . As found by TEM, the mean nanoparticle diameter was  $15.2 \pm 1.2$  nm (Figure 1). The per-ml number of particles at  $A_{520}=1$  was  $1.6 \times 10^{12}$ . Earlier work by us showed that spherical GNPs with a mean diameter of 15 nm are optimal for use in immunization [40].

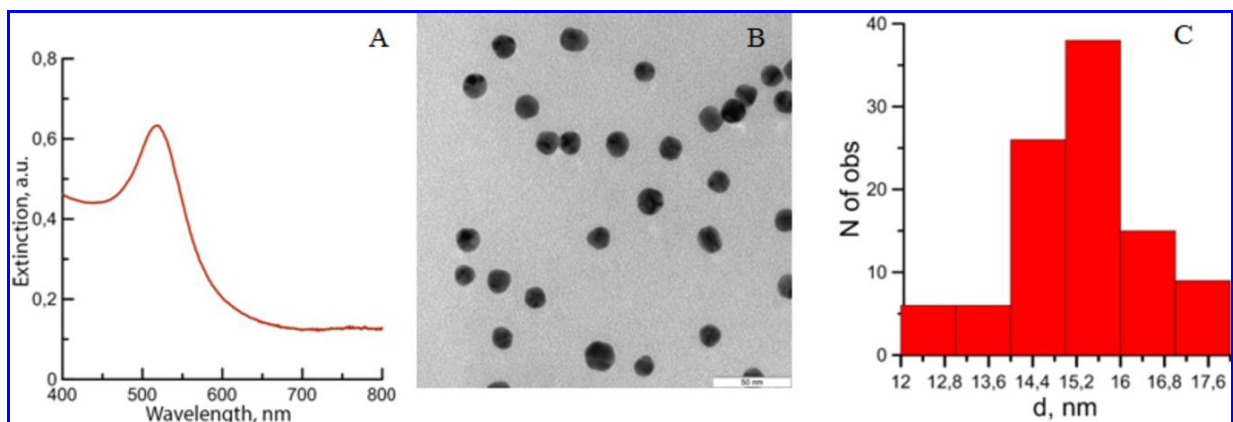


**Figure 1:** Characterization of GNPs: absorption spectrum (A), TEM image (B), and size distribution (DLS data) (C)

### Characterization of antigens

Figure 2 shows the results for the content of the main HSPs in the whole-cell lysate of MH22a cells. The results were obtained by dot blot immunoassay by using a set of rabbit anti-HSP polyclonal antibodies. As can be seen, the lysate of heated MH22a

cells contained all main HSPs, including GRP94, HSP 90 kDa alpha B1 (HSP90aB1), HSP 70 kDa 1A (HSPA1A), HSP 70 kDa 1B (HSPA1B), and HSP 27 kDa.

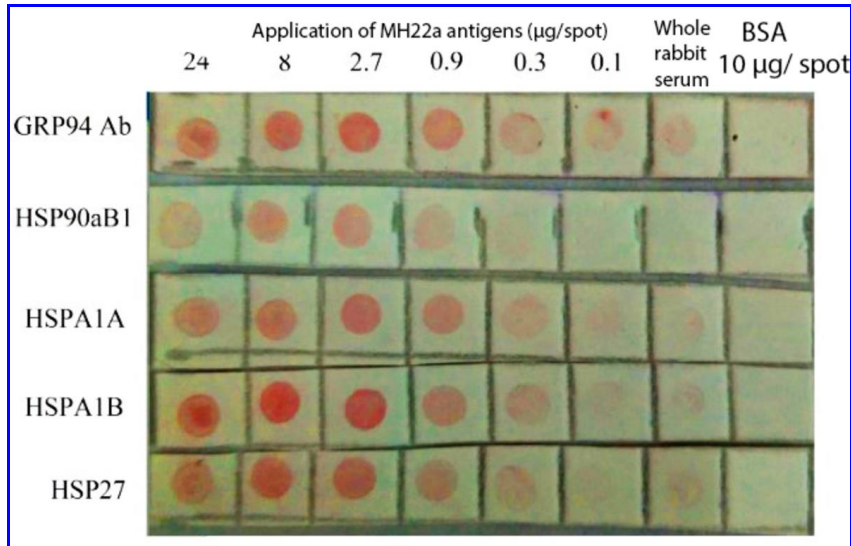


**Figure 2:** Identification of HSPs in whole-cell lysate of MH22a by dot blot immunoassay

### Immunization results

Table 1 shows the obtained antibody titers. The highest titer (1:10666 on average; maximum titer, 1:12800) was produced in mice immunized with the GNP–antigen–CFA complex. Immunization with the antigen and GNPs separately gave average titers of 1:1200 (maximal titer, 1:1600) and 1:1066 (maximal titer, 1:1600), respectively. The average titer in mice immunized with the GNP–antigen conjugate was 1:366 (maximal titer, 1:800). When mice were immunized with GNPs alone, the presence of an antibody titer and the ability of antibodies to bind to the cellular antigen were probably related to the immune response of the animals to the tumor-cell transplantation. In the blot assay of the MH22a HSPs, the resulting antiserum specifically recognized peptides ranging in size from 25 to 66 kDa.

**Table 1:** Antibody titers produced by different immunization schemes after tumor-cell transplantation

Immunogen	Antibody titer			Student's <i>t</i> test relative to the antigen ( $p \leq 0.05$ )
	Average titer	Maximal titer	Average titer ( $\log_2$ )	
Antigen	1: 1200	1:1600	10.14±0.9	
GNPs + antigen	1:366	1:800	8.14±2.03	0.092
GNPs + antigen + CFA	1:10666	1:12800	13.31±0.8	0.00062
GNPs	1:1066	1:1600	9.997±0.8	0.074

The specificity of the antisera obtained from the immunized mice was examined by dot immunoassay (Figure 3). Note that the sera interacted mainly with the MN22a cell antigens. But the sera obtained from the mice immunized with the GNP–antigen–CFA complex and those immunized with GNPs alone gave a small crossover with the HeLa cell antigens.

Figure 4 shows the results for the respiratory activity of peritoneal macrophages isolated from animals of different groups after immunization and subsequent tumor transplantation. As found by MTT test, there were no large differences between the groups of animals injected with the antigen alone, the GNP–antigen conjugate, and the GNP–antigen–CFA complex. However, in the animals injected with GNPs alone, the respiratory activity of peritoneal macrophages decreased slightly.

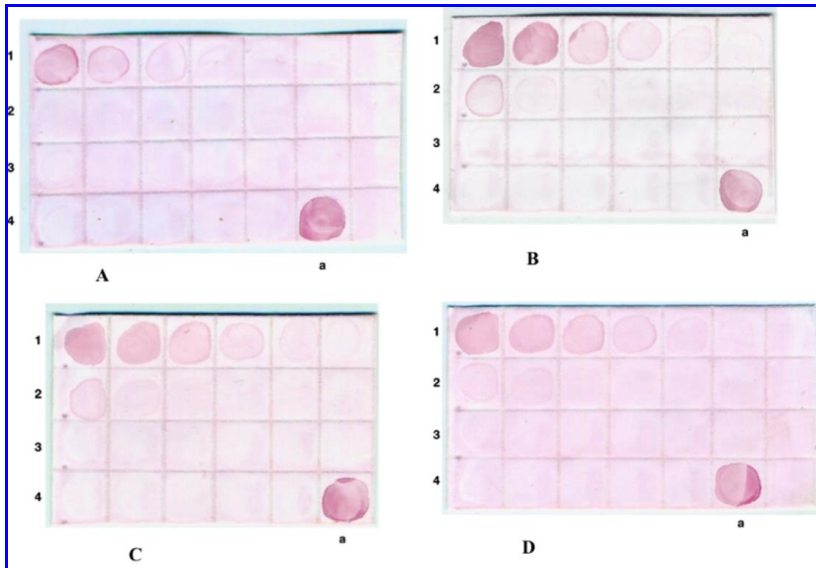


**Figure 3:** Dot immunoassay of antigens with antisera from mice immunized with antigen (A), GNPs + antigen (B), GNPs + antigen + CFA (C), and GNPs (D). 1, MN22a. 2, HeLa. 3, SPEV-2. 4a, serum (positive control)

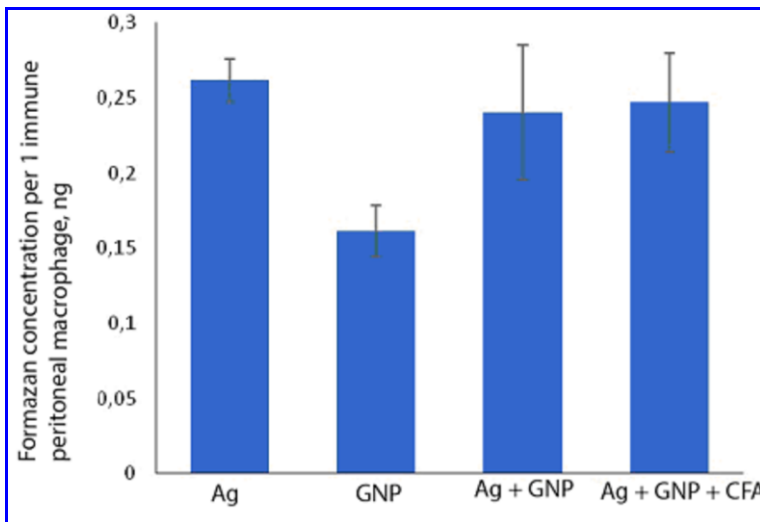


**Figure 4:** Changes in respiratory activity of peritoneal macrophages in mice immunized by different schemes

Figure 5 shows the results for the content of proinflammatory cytokines in the sera of mice after immunization and subsequent tumor transplantation. In the mice immunized with the GNP–antigen conjugate, the production of proinflammatory

cytokines was significantly reduced, as compared to that in the other groups. IFN- $\gamma$  production decreased by an average of 79%; IL-6 production, by an average of 80%; and IL-1 production, by an average of 57%. In the other groups of mice, no significant differences were noted between the amounts of proinflammatory cytokines produced.

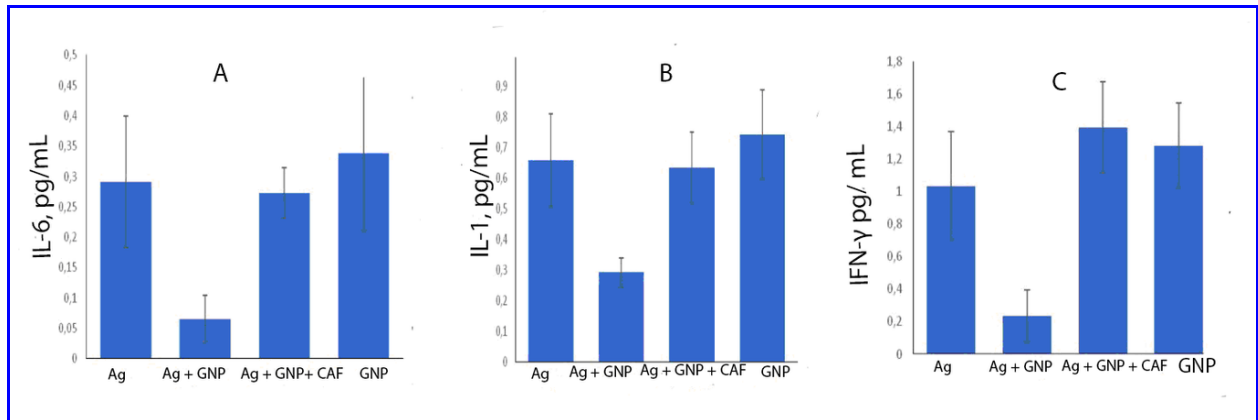


**Figure 5:** Content of IL-6 (A), IFN- $\gamma$  (B), and IL-1 (C) in sera of mice after immunization and subsequent tumor transplantation

### Tumor formation results

Seven days after the last immunization, the mice received transplants of MH22a tumor cells. In groups 1, 3, and 4, variously sized tumors (0.5–2.5 cm; Figure 6A) were present in all animals. On histological examination of the tumors, no hepatic lobule structure, characteristic of the liver parenchyma, was observed. Nested cell clusters were well visualized. The tumor cells were morphologically similar to hepatocytes but were larger than them; they were polygonal, with globular nuclei and clearly defined karyosomes. Between neighboring tumor cells there were ring-shaped structures characteristic of hepatomas (Figure 6B). Yet, no tumors were observed at the injection site in any group 2 mouse (GNPs + Ag). Only one mouse had a small lump on day 21, but the lump disappeared on day 24. In groups 1, 3, and 4, the

transplanted tumor cells survived 100%. Tumors appeared on day 5. Tumor sizes were measured on days 10 and 24.

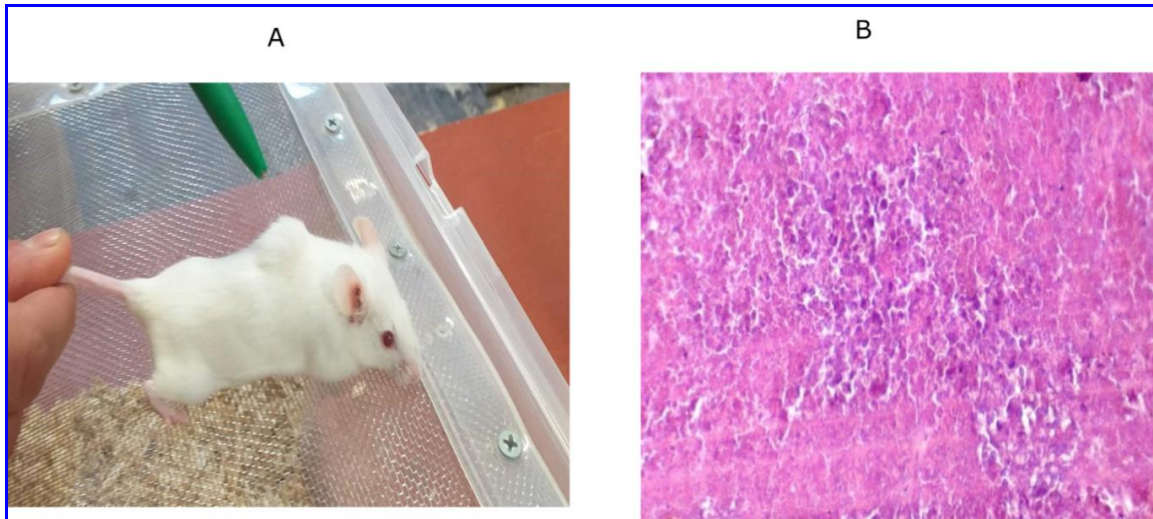


**Figure 6:** Appearance of a mouse with a transplanted tumor on day 24 after transplantation (**A**), photograph by S. Staroverov. Histological section of the tumor on day 24 after transplantation (**B**). Staining with hematoxylin–eosin,  $\times 300$

When the growth dynamics were constant, the tumor size in the infected mice was maximal on day 24. But tumor weight varied depending on the immunization method. Specifically, tumor weight was the largest in the animals immunized with the GNP–antigen–CFA complex—0.287 g, which is actually twice as large as the values obtained for the animals immunized with the antigen and GNPs alone (Figures 7 and 8).

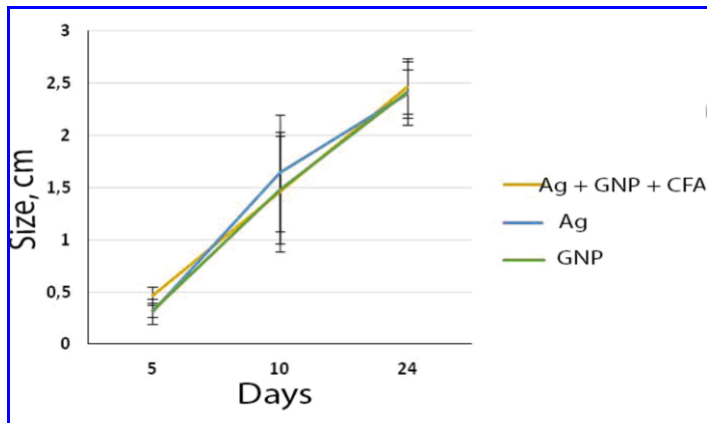


**Figure 7:** Tumor growth dynamics

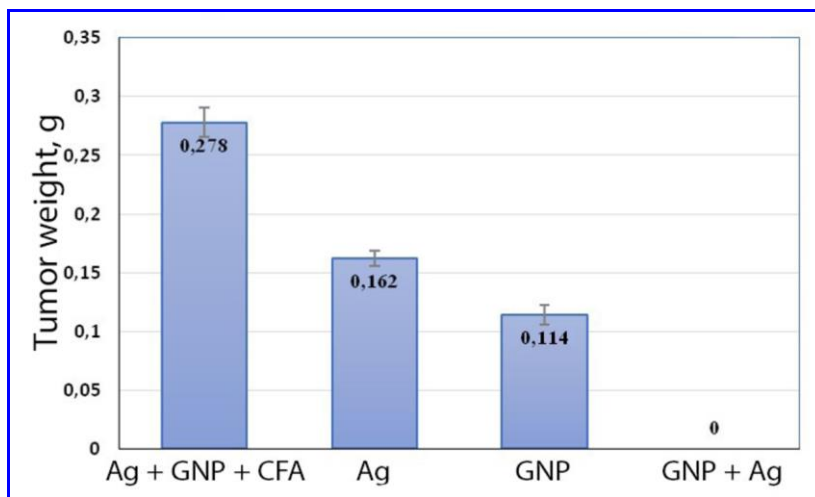


**Figure 8:** Tumor weight after euthanasia

## Discussion

Analysis of the results shows that animal immunization with the GNP–antigen conjugate prevents tumor formation after cancer cell transplantation. This is in spite of the fact that the antibody titer produced by conjugate immunization was the lowest. This may be because in this case, immunization produces a Th1-dependent immune response. It is accompanied by the elaboration of IFN- $\gamma$ , IL-2, and TNF- $\alpha$ , which affect the production of opsonizing and complement-binding antibodies by B-cells, the activation of macrophages, cytotoxicity, and the induction of cellular immunity.

Immune responses dominated by Th1 cells mostly cause phagocyte-dependent inflammation [41, 42]. The number of T cells, especially activated CD8<sup>+</sup> cytotoxic T cells and Th1 cells, correlates with better survival in some cancers, including invasive colorectal cancer, melanoma, multiple myeloma, and pancreatic cancer [43].

In the mice injected with the GNP–antigen–CFA complex, tumor induction could have been due to an inflammatory process in the tumor microenvironment that could have been caused by immunization with CFA and by increased contents of IL-1 $\beta$ , IL-6, IL-8, and monocyte chemoattractant protein-1 (MCP-1), observed in breast cancer patients [44,45]. It has been suggested that these mediators can directly promote the proliferation and invasion of breast cancer cells or can participate in angiogenesis, which is important for breast cancer development and progression [46].

Kitamura et al. [47] reported that IL-6 suppresses major histocompatibility complex (MHC) class II expression on Th1 cells, inhibiting IFN- $\gamma$  and IL-2 secretion. They noted that in this case, the cancer cells evaded antitumor immunological effects through the reduction in cytotoxic T lymphocyte activity. This has also been pointed out in studies on the relationship between IL-6 and gastrointestinal and other cancers, and a role was found for IL-6 in the development and maintenance of neoplastic cells. Gastric cancer cells secrete IL-6, and increased serum and tumor-tissue amounts of IL-6 possibly regulate tumor growth and development. Also, increased amounts of inflammatory mediators such as TNF- $\alpha$ , C-reactive protein, and IL-6 have been found in the sera of hepatocellular carcinoma patients [48,49].

## **CONCLUSION**

Recent years have seen intense development of effective adjuvants for antitumor immunotherapy. In particular, HSPs [50,51] and GNPs of various sizes and shapes

have been proposed as such [52-54]. Here we used both of these adjuvants to examine the part they play in the induction of antitumor immunity in laboratory mice. We prepared conjugates based on 15-nm GNPs and thermostable antigens isolated from MH22a murine hepatoma cells. BALB/c mice were immunized by different schemes, and then they received transplants of MH22a cells. The mice immunized with the GNP–antigen conjugate showed no signs of tumor growth for 24 days. None of the mice in this group developed a tumor, whereas mice in all the other groups did. The mice immunized with the nanoconjugate had the lowest antibody titer. They also showed significantly decreased production of the INF- $\gamma$ , IL-6, and IL-1 proinflammatory cytokines.

This study has shown that it is possible in principle to use GNPs in combination with HSPs for antitumor vaccination. The results suggest that anticancer vaccines can be largely improved by including GNPs as additional adjuvants. The next stage of research could be to design and test therapeutic vaccines based on HSPs and colloidal gold.

## **Experimental**

### **Preparation of GNPs**

Gold nanospheres were made as described by Frens [55], by reducing H<sub>Au</sub>Cl<sub>4</sub> with sodium citrate. A 240-ml portion of deionized water was heated to boiling in an Erlenmeyer flask fitted with a water-cooled reflux tube. This was followed by the addition to the flask of 2.5 ml of 1% aqueous H<sub>Au</sub>Cl<sub>4</sub> (Sigma–Aldrich, USA) and 7.75 ml of 1% sodium citrate (Fluka, Switzerland). The mixture was vigorously stirred. The mean particle size was examined by spectrophotometry, transmission electron microscopy (TEM), and dynamic light scattering (DLS).

### **Preparation of conjugates**

A 150- $\mu$ l portion of staphylococcal protein A (concentration, 1 mg/ml) and 25 ml of colloidal gold solution ( $A_{518} = 1$ ) were mixed. The mixture was stirred for 10 min. Then 500  $\mu$ l of 1% PEG-20,000 was added to the reaction mixture, and the mixture was stirred for another 5 min. The samples were centrifuged at 12,000 g for 40 min, and the supernatant liquid was decanted. The sediment was redissolved in a buffer composed of 10 mM PBS, 0.02 M  $\text{NaN}_3$ , 0.02% PEG-20,000, and 30% glycerol so that the  $A_{518}$  of the sample was 5. The conjugates were stored at  $-20^\circ\text{C}$ . GNP–tumor-antigen conjugates were made in the same way.

### **Culturing of cells**

MH22a murine hepatoma cells, HeLa cervical carcinoma cells, and SPEV-2 porcine embryonic kidney cells were used. All cells were obtained from the Russian Collection of Cell Cultures of the Russian Academy of Sciences' Institute of Cytology, St. Petersburg, Russia.

Cells were grown on Dulbecco's modified Eagle's medium (DMEM) with 10% fetal bovine serum, 100 units/ml penicillin, 100  $\mu$ g/ml streptomycin, and 292  $\mu$ g/ml L-glutamine. They were grown in sterile adhesive-culture bottles until monolayers were formed.

### **Isolation of the total HSP fraction**

After monolayers were formed, HSPs were isolated as described [56,57]. The culture bottle with the MH22a monolayer was heated at  $42^\circ\text{C}$  for 1 h and incubated at  $37^\circ\text{C}$  for 2 h. The cells were lysed, and the bottle was gently washed four times with 10 ml of heated Hanks solution. Then, 15 ml of DMEM containing 4 mM glutamine and 2 mM PMSF was added. After the bottle was shaken at  $37^\circ\text{C}$  for 1 h and was washed, it received 10 ml of Cytomix buffer (120 mM KCl, 0.15 mM  $\text{CaCl}_2$ , 2 mM EDTA, 5 mM  $\text{MgCl}_2$ , 10 mM  $\text{K}_2\text{HPO}_4/\text{KH}_2\text{PO}_4$ , 25 mM HEPES, 2 mM PMSF, pH 8.0) and, finally,

was frozen at -20°C and thawed at 37°C. This procedure was repeated three times. The suspension was then transferred to a centrifuge tube and spun at 10,000 g for 15 min. Alternatively, cells were removed from the monolayer by trypsin treatment and  $7 \times 10^6$  tumor cells were lysed as described above. The resultant samples were clarified by centrifugation at 20,000 g for 20 min. Protein was measured by the Bradford method and was frozen at -70°C.

The cell lysate was then precipitated with ammonium sulfate to 40% saturation, and the precipitate was spun at 20,000 g for 20 min at 4°C. The resulting supernatant liquid was precipitated with ammonium sulfate to a final saturation of 80%, and the precipitate was spun at 20,000 g for 20 min at 4°C. The sediment obtained after the second centrifugation was dissolved in 4 ml distilled water and dialyzed against 0.2 M PBS, pH 7.2, at 4°C for 48 h with frequent buffer changes. Antigens from HeLa and SPEV-2 cells were isolated in the same manner. The resultant extracts were used for further chromatographic purification.

### **Chromatographic purification of antigens**

Antigens were purified by ion-exchange chromatography on a Toyopearl DEAE-650 column (Sigma, USA), by using an NGC Quest 10 chromatograph (Bio-Rad, USA). The phase was equilibrated with 0.05 M Tris-HCl, pH 7.5. The equilibrated sample (100  $\mu$ L), containing 240  $\mu$ g protein, was applied to the column. The eluates were collected as fractions by using a stepwise gradient of 0 to 0.5 M NaCl. The absorbance of the eluates was monitored at 280 nm with a Spectronic-21 spectrophotometer (Thermo Scientific, USA).

### **Dot blot immunoassay**

The dot immunoassay was run as follows [58]: Extracts from MH22a cells were applied as a series of spots onto a Western S polyvinylidene fluoride membrane (Millipore, USA). The membrane was blocked for 1 h with 2% fat-free powdered milk

diluted in 10 mM PBS, pH 7.2, and was then incubated for 1 h in a solution of antibodies prediluted 1:150. The isolated HSPs were identified by using mouse polyclonal antibodies against GRP94 (Affinity Bioscience, Germany), HSP 90 kDa alpha B1 (HSP90aB1), HSP 70 kDa 1A (HSPA1A), HSP 70 kDa 1B (HSPA1B), and HSP 27 kDa (Cloud-Clone, USA). When there was a biospecific interaction, the antibodies bound to the antigen adsorbed on the membrane. The membrane was then washed free of nonspecifically bound antibodies and was immersed in a solution of GNPs conjugated to staphylococcal protein A ( $A_{518}=1$ ). After 5–60 min, the binding of the conjugate to the antigen–antibody complex was observable visually as a series of red spots.

### **Western blotting**

First, sodium dodecyl sulfate–polyacrylamide gel electrophoresis (SDS–PAGE) was done according to Laemmli [59]. Molecular weight marker protein standards (Sigma, USA) were included in each gel. After electrophoresis, the gels were stained with Coomassie Brilliant Blue R-250 (Sigma, USA). For Western blotting, the electrophoresed samples were transferred to a Western S membrane with a semidry blotter and the membrane was incubated for 1 h in a blocking buffer containing 10 mM PBS, 0.1% Tween 20, and 5% fat-free powdered milk. Finally, the membrane was incubated for 1 h in an antibody-containing serum solution and the reaction results were detected with GNPs conjugated to staphylococcal protein A ( $A_{518} = 1$ ).

### **Examination of antitumor efficacy of GNP–antigen conjugates**

GNPs complexed with thermostable antigens derived from the MH22a whole-cell lysate were used to immunize BALB/c white mice. The animals were divided into six groups of five in each. Group 1 received a PBS solution of the antigen (3  $\mu$ g; 250  $\mu$ L); group 2, the GNP–antigen conjugate (3  $\mu$ g; 250  $\mu$ L); group 3, the conjugate emulsified 1:1 with complete Freund's adjuvant (CFA) (3  $\mu$ g; 500  $\mu$ L); and group 4, a

solution of GNPs (250  $\mu$ L). The animals were immunized intraperitoneally by two injections with an interval of 10 days in between. Seven days after the last immunization, the animals received transplants of MH22a tumor cells. These were injected into the withers at  $1 \times 10^9$  cells/mouse. The first signs of tumors appeared 14 days after infection; on day 21, the tumors were most clearly visible. On day 24, the animals were killed and blood was drawn to determine the antibody titer and the interleukin content. In addition, peritoneal cells were isolated to measure respiratory activity (MTT test) and tumor histology was evaluated.

Animals were cared for and handled in accordance with the Guide for the Care and Use of Laboratory Animals, the European Convention for the Protection of Vertebrate Animals Used for Experimental and Other Scientific Purposes, and the legislation of the Russian Federation. The use of the animals was also approved by the institution where the experiments were performed.

Work with laboratory animals was carried out at the Federal State Budgetary Educational University of Higher Education "Saratov State Agrarian University named after N.I. Vavilov". The permissive document is the charter of the university, approved by the order of the Ministry of Agriculture of the Russian Federation dated June 18, 2015 No. 66-u.

### **Enzyme-linked immunosorbent assay**

The antibody titer was estimated by enzyme-linked immunosorbent assay (ELISA) with horseradish peroxidase-labeled secondary antibodies against mouse IgG (Jackson ImmunoResearch, UK) [60]. The reaction results were recorded on a Plate Screen analyzer (Hospitex Diagnostics, Italy). Animal sera were diluted 10-fold and then doubly titrated. The serum interleukin concentrations were measured by ELISA with reagent kits for IL-1 $\beta$ , IL-6, and IFN- $\gamma$  (Vector-Best, Russia).

### **Examination of cellular respiratory activity**

The respiratory activity of peritoneal macrophages was measured by the ability of the cells to reduce nitroreductase [3-(4,5-dimethylthiazol-2-yl)-2,5-diphenyltetrazolium bromide] to formazan (MTT test) [61]. Experimental and control cells (200  $\mu$ l of each kind) were added to the wells of a microtitration plate, and the plate was placed in a CO<sub>2</sub> incubator. After 72 h, 20  $\mu$ l of 0.5% MTT solution was added to all wells and the plate was incubated for another 3.5 h. An MTT stock solution (5 mg/ml) was made with PBS and stored at 4°C in a dark vessel for no more than 2 weeks. A 165–170- $\mu$ l portion of the supernatant liquid was carefully taken from the wells, and 150  $\mu$ l of DMSO was added to dissolve the formed formazan crystals. The contents of the wells were carefully pipetted; alternatively, a microshaker was used to shake the plates. The absorbance of the solution was measured on a Spark-10M microplate reader (Tecan, Switzerland) at 560 nm. The proliferation coefficient was calculated from the formula  $K = A_{\text{exp}}/A_{\text{ctrl}}$ .

### **Pathomorphological studies**

The animals were killed by cervical dislocation under anesthesia. Tumor size was measured with a micrometer with a division value of 0.1 mm. For histological studies, whole tumors were placed in a container with a 10% neutral aqueous buffered solution of formaldehyde, 96° alcohol, and Carnoy's fixative. From the fixed tumors, paraffin blocks (Histomix embedding medium; BioVitrum, Russian Federation) were made by standard procedures. Sections were cut on a MICROM HM 450 sliding microtome (Germany).

For microscopic observation, sections were stained with hematoxylin–eosin by the Ehrlich method. The stained sections were embedded into Canadian balm (Panreac, Spain) under a coverslip and were examined with a Micromed S-1 biological

microscope (Biomed, Russia). Microphotographs were taken with a CANON PowerShot A460 IS camera (Canon, Japan).

## Statistics

The results were statistically processed by the standard procedures integrated into Excel 2007 software (Microsoft Corp., USA). After the arithmetic mean and the standard deviation for a given data sample had been found, we determined the standard error of the arithmetic mean and its confidence limits with account taken of Student's  $t$  coefficient ( $n, p$ ) [number of measurements  $n = 3$ , significance level = 95% ( $p = 0.05$ )]. These results are presented as histograms. The significance of differences between individual samples was evaluated by a two-sample unpaired Student's  $t$  test with unequal variances. Differences were considered significant when the experimentally found  $p_{\text{exp}}$  value was  $\leq 0.05$ .

## Acknowledgements

We thank Mr. D.N. Tychinin for his help in preparation of the manuscript. This work was supported by the Russian Science Foundation [Grant No. 19-14-00077].

## REFERENCES

1. Waldmann, T. A. *Cold Spring Harb. Perspect. Biol.* **2018**, *10*, a028472.  
doi:10.1101/cshperspect.a028472
2. Robert, C. *Nat. Commun.* **2020**, *11*, 3801. doi:10.1038/s41467-020-17670-y
3. Rohaan, M. W.; Wilgenhof, S.; Haanen, J. B. A. G. *Virchows Arch.* **2019**, *474*, 449–461.  
doi:10.1007/s00428-018-2484-0
4. Apostolopoulos, V. *Cancers* **2019**, *11*, 1041. doi:10.3390/cancers11081041
5. Finn, O. J. *Nat. Rev. Immunol.* **2003**, *3*, 630–641. doi:10.1038/nri1150

6. Lou, J.; Zhang, L.; Zheng, G. *Adv. Ther.* **2019**, *2*, 1800128. doi:10.1002/adtp.201800128
7. Wang, X.; Li, X.; Ito, A.; Watanabe, Y.; Sogo, Y.; Tsuji, N. M.; Ohno, T. *Angew. Chem.* **2016**, *55*, 1899–1903. doi:10.1002/anie.201506179
8. Luo, M.; Wang, H.; Wang, Z.; Cai, H.; Lu, Z.; Li, Y.; Du, M.; Huang, G.; Wang, C.; Chen, X.; Porembka, M. R.; Lea, J.; Frankel, A. E.; Fu, Y. X.; Chen, Z. J.; Gao, J. *Nat. Nanotechnol.* **2017**, *12*, 648–654. doi:10.1038/nnano.2017.52
9. Zhou, L.; Hou, B.; Wang, D.; Sun, F.; Song, R.; Shao, Q.; Wang, H.; Yu, H.; Li, Y. *Nano Lett.* **2020**, *20*, 4393–4402. doi:10.1021/acs.nanolett.0c01140
10. Salazar-González, J. A.; González-Ortega, O.; Rosales-Mendoza, S. *Expert Rev. Vaccines* **2015**, *14*, 1197–1211. doi:10.1586/14760584.2015.1064772
11. Dykman, L. A.; Khlebtsov, N. G. *Chem. Sci.* **2017**, *8*, 1719–1735. doi:10.1039/c6sc03631g
12. Alkilany, A. M.; Murphy, C. J. *J. Nanopart. Res.* **2010**, *12*, 2313–2333. doi:10.1007/s11051-010-9911-8
13. Dykman, L. A.; Khlebtsov, N. G. *Russ. Chem. Rev.* **2019**, *88*, 229–247. doi:10.1070/RCR4843
14. Dreaden, E. C.; Alkilany, A. M.; Huang, X.; Murphy, C. J.; El-Sayed, M. A. *Chem. Soc. Rev.* **2012**, *41*, 2740–2779. doi:10.1039/c1cs15237h
15. Dykman, L. A. *Expert Rev. Vaccines* **2020**, *19*, 465–477. doi:10.1080/14760584.2020.1758070
16. Burygin, G. L.; Abronina, P. I.; Podvalnyy, N. M.; Staroverov, S. A.; Kononov, L. O.; Dykman, L. A. *Beilstein J. Nanotechnol.* **2020**, *11*, 480–493. doi:10.3762/bjnano.11.39
17. Brinãs, R. P.; Sundgren, A.; Sahoo, P.; Morey, S.; Rittenhouse-Olson, K.; Wilding, G. E.; Deng, W.; Barchi, J. J., Jr. *Bioconjug. Chem.* **2012**, *23*, 1513–1523. doi:10.1021/bc200606s
18. Parry, A.L.; Clemson, N. A.; Ellis, J.; Bernhard, S. S.; Davis, B. G.; Cameron, N. R. *J. Am. Chem. Soc.* **2013**, *135*, 9362–9365. doi:10.1021/ja4046857

19. Cai, H.; Degliangeli, F.; Palitzsch, B.; Gerlitzki, B.; Kunz, H.; Schmitt, E.; Fiammengo, R.; Westerlind, U. *Bioorg. Med. Chem.* **2016**, *24*, 1132–1135. doi:10.1016/j.bmc.2016.01.044
20. Mocan, T.; Matea, C.; Tabaran, F.; Iancu, C.; Orasan, R.; Mocan, L. *J. Cancer* **2015**, *6*, 583–592. doi:10.7150/jca.11567
21. Liu, Y.; Wang, Z.; Yu, F.; Li, M.; Zhu, H.; Wang, K.; Meng, M.; Zhao, W. *Int. J. Nanomedicine* **2021**, *16*, 403–420. doi:10.2147/IJN.S273883
22. Almeida, J. P. M.; Lin, A. Y.; Figueroa, E. R.; Foster, A. E.; Drezek, R. A. *Small* **2015**, *11*, 1453–1459. doi:10.1002/sml.201402179
23. Ahn, S.; Lee, I. H.; Kang, S.; Kim, D.; Choi, M.; Saw, P. E.; Shin, E. C.; Jon, S. *Adv. Healthc. Mater.* **2014**, *3*, 1194–1199. doi:10.1002/adhm.201300597
24. Gulla, S.K.; Rao, B.R.; Moku, G.; Jinka, S.; Nimmu, N.V.; Khalid, S.; Patra, C. R.; Chaudhuri, A. *Biomater. Sci.* **2019**, *7*, 773–778. doi:10.1039/c8bm01272e
25. Gulla, S.K.; Kotcherlakota, R.; Nimushakavi, S.; Nimmu, N.V.; Khalid, S.; Patra, C. R.; Chaudhuri, A. *ACS Omega* **2018**, *3*, 8663–8676. doi:10.1021/acsomega.8b01051
26. Zhang, Y.; Fu, J.; Shi, Y.; Peng, S.; Cai, Y.; Zhan, X.; Song, N.; Liu, Y.; Wang, Z.; Yu, Y.; Wang, Y.; Shi, Q.; Fu, Y.; Yuan, K.; Zhou, N.; Joshi, R.; Ichim, T. E.; Min, W. *Int. J. Cancer* **2018**, *143*, 2039–2052. doi:10.1002/ijc.31588
27. He, J.-s.; Liu, S.-j.; Zhang, Y.-r.; Chu, X.-d.; Lin, Z.-b.; Zhao, Z.; Qiu, S.-h.; Guo, Y.-g.; Ding, H.; Pan, Y.-l.; Pan, J.-h. *Front. Pharmacol.* **2021**, *12*, 687399. doi:10.3389/fphar.2021.687399
28. Shevtsov, M.; Multhoff, G. *Front. Immunol.* **2016**, *7*, 171. doi:10.3389/fimmu.2016.00171
29. Schlesinger, M. J. *J. Biol. Chem.* **1990**, *265*, 12111–12114.
30. Murshid, A.; Gong, J.; Stevenson, M. A.; Calderwood, S. K. *Expert Rev. Vaccines* **2011**, *10*, 1553–1568. doi:10.1586/erv.11.124
31. Multhoff, G.; Pfister, K.; Gehrmann, M.; Hantschel, M.; Gross, C.; Hafner, M.; Hiddemann, W. *Cell Stress Chaperones* **2001**, *6*, 337–344. doi:10.1379/1466-1268(2001)006<0337:AMHPSN>2.0.CO;2

32. Basu, S.; Srivastava, P. K. *Cell Stress Chaperones* **2000**, *5*, 443–451. doi:10.1379/1466-1268(2000)005<0443:hsptfo>2.0.co;2
33. Tsan, M. F.; Gao, B. *Am. J. Physiol. Cell Physiol.* **2004**, *286*, C739–C744.  
doi:10.1152/ajpcell.00364.2003
34. Mazzaferro, V.; Coppa, J.; Carrabba, M. G.; Rivoltini, L.; Schiavo, M.; Regalia, E.; Mariani, L.; Camerini, T.; Marchianò, A.; Andreola, S.; Camerini, R.; Corsi, M.; Lewis, J. J.; Srivastava, P. K.; Parmiani, G. *Clin. Cancer Res.* **2003**, *9*, 3235–3245.
35. Maki, R. G.; Livingston, P. O.; Lewis, J. J.; Janetzki, S.; Klimstra, D.; Desantis, D.; Srivastava, P. K.; Brennan, M. F. *Dig. Dis. Sci.* **2007**, *52*, 1964–1972.  
doi:10.1007/s10620-006-9205-2
36. Pilla, L.; Patuzzo, R.; Rivoltini, L.; Maio, M.; Pennacchioli, E.; Lamaj, E.; Maurichi, A.; Massarut, S.; Marchianò, A.; Santantonio, C.; Tosi, D.; Arienti, F.; Cova, A.; Sovena, G.; Piris, A.; Nonaka, D.; Bersani, I.; Di Florio, A.; Luigi, M.; Srivastava, P. K.; Hoos, A.; Santinami, M.; Parmiani, G. *Cancer Immunol. Immunother.* **2006**, *55*, 958–968.  
doi:10.1007/s00262-005-0084-8
37. Testori, A.; Richards, J.; Whitman, E.; Mann, G. B.; Lutzky, J.; Camacho, L.; Parmiani, G.; Tosti, G.; Kirkwood, J. M.; Hoos, A.; Yuh, L.; Gupta, R.; Srivastava, P. K. *J. Clin. Oncol.* **2008**, *26*, 955–962. doi:10.1200/JCO.2007.11.9941
38. Ampie, L.; Choy, W.; Lamano, J. B.; Fakurnejad, S.; Bloch, O.; Parsa, A. T. *J. Neurooncol.* **2015**, *123*, 441–448. doi:10.1007/s11060-015-1837-7
39. Shevtsov, M. A.; Nikolaev, B. P.; Yakovleva, L. Y.; Parr, M. A.; Marchenko, Y. Y.; Eliseev, I.; Yudenko, A.; Dobrodumov, A. V.; Zlobina, O.; Zhakhov, A.; Ischenko, A. M.; Pitkin, E.; Multhoff, G. *J. Control. Release* **2016**, *220*, 329–340. doi:10.1016/j.jconrel.2015.10.051
40. Dykman, L. A.; Staroverov, S. A.; Fomin, A. S.; Khanadeev, V. A.; Khlebtsov, B. N.; Bogatyrev, V. A. *Int. Immunopharmacol.* **2018**, *54*, 163–168.  
doi:10.1016/j.intimp.2017.11.008
41. DeNardo, D. G.; Barreto, J. B.; Andreu, P.; Vasquez, L.; Tawfik, D.; Kolhatkar, N.; Coussens, L. M. *Cancer Cell* **2009**, *16*, 91–102. doi:10.1016/j.ccr.2009.06.018

42. Laghi, L.; Bianchi, P.; Miranda, E.; Balladore, E.; Pacetti, V.; Grizzi, F.; Allavena, P.; Torri, V.; Repici, A.; Santoro, A.; Mantovani, A.; Roncalli, M.; Malesci, A. *Lancet Oncol.* **2009**, *10*, 877–884. doi:10.1016/S1470-2045(09)70186-X
43. Grivennikov, S. I.; Greten, F. R.; Karin, M. *Cell* **2010**, *140*, 883–899.  
doi:10.1155/2017/6027305
44. Goldberg, J. E.; Schwertfeger, K. L. *Curr. Drug Targets* **2010**, *11*, 1133–1146.  
doi:10.2174/138945010792006799
45. Gilbert, C. A.; Slingerland, J. M. *Annu. Rev. Med.* **2013**, *64*, 45–57. doi:10.1146/annurev-med-121211-091527
46. Nicolini, A.; Carpi, A.; Rossi, G. *Cytokine Growth Factor Rev.* **2006**, *17*, 325–337.  
doi:10.1016/j.cytogfr.2006.07.002
47. Kitamura, H.; Ohno, Y.; Toyoshima, Y.; Ohtake, J.; Homma, S.; Kawamura, H.; Takahashi, N.; Taketomi, A. *Cancer Sci.* **2017**, *108*, 1947–1952. doi:10.1111/cas.13332
48. Vainer, N.; Dehlendorff, C.; Johansen, J. S. *Oncotarget* **2018**, *9*, 29820–29841.  
doi:10.18632/oncotarget.25661
49. Wang, H.; Liu, J.; Hu, X.; Liu, S.; He, B. *Med. Sci. Monit.* **2016**, *22*, 3694–3704.  
doi:10.12659/msm.899773
50. Lei, Y.; Zhao, F.; Shao, J.; Li, Y.; Li, S.; Chang, H.; Zhang, Y. *Peer J.* **2019**, *6*, e6185.  
doi:10.7717/peerj.6185
51. Banstola, A.; Jeong, J.-H.; Yook, S. *Acta Biomater.* **2020**, *114*, 16–30.  
doi:10.1016/j.actbio.2020.07.063
52. Chauhan, A.; Khan, T.; Omri, A. *Int. J. Mol. Sci.* **2021**, *22*, 8037.  
doi:10.3390/ijms22158037
53. Zhou, L.; Liu, H.; Liu, K.; Wei, S. *Front. Pharmacol.* **2021**, *12*, 739481.  
doi:10.3389/fphar.2021.739481

54. Toraskar, S.; Chaudhary, P. M.; Kikkeri, R. Nanoparticle shape governs immunomodulation of MUC1 antigen to develop anti-cancer vaccine, bioRxiv, 2021. <https://www.biorxiv.org/content/10.1101/2021.09.29.460739v1>. doi:10.1101/2021.09.29.460739.
55. Frens, G. *Nat. Phys. Sci.* **1973**, *241*, 20–22. doi:10.1038/physci241020a0
56. Aguilera, R.; Saffie, C.; Tittarelli, A.; Gonzalez, F. E.; Ramírez, M.; Reyes, D.; Pereda, C.; Hevia, D.; García, T.; Salazar, L.; Ferreira, A.; Hermoso, M.; Mendoza-Naranjo, A.; Ferrada, C.; Garrido, P.; Lopez, M. N.; Salazar-Onfray, F. *Clin. Cancer Res.* **2011**, *17*, 2474–2483. doi:10.1158/1078-0432.CCR-10-2384
57. Skarga, Y.; Vrublevskaya, V.; Evdokimovskaya, Y.; Morenkov, O. *Biomed. Chromatogr.* **2009**, *23*, 1208–1216. doi:10.1002/bmc.1245
58. Dykman, L. A.; Bogatyrev, V. A. *Biochemistry (Moscow)*. **1997**, *62*, 350–356.
59. Laemmli, U. K. *Nature* **1970**, *227*, 680–685. doi:10.1038/227680a0
60. Shah, K.; Maghsoudlou, P. *Br. J. Hosp. Med.* **2016**, *77*, C98–C101. doi:10.12968/hmed.2016.77.7.C98
61. Bernas, T.; Dobrucki, J. W. *Arch. Biochem. Biophys.* **2000**, *380*, 108–116. doi:10.1006/abbi.2000.1907